iScience

CellPress
OPEN ACCESS

Article

Controllable synthesis of high-quality two-dimensional tellurium by a facile chemical vapor transport strategy

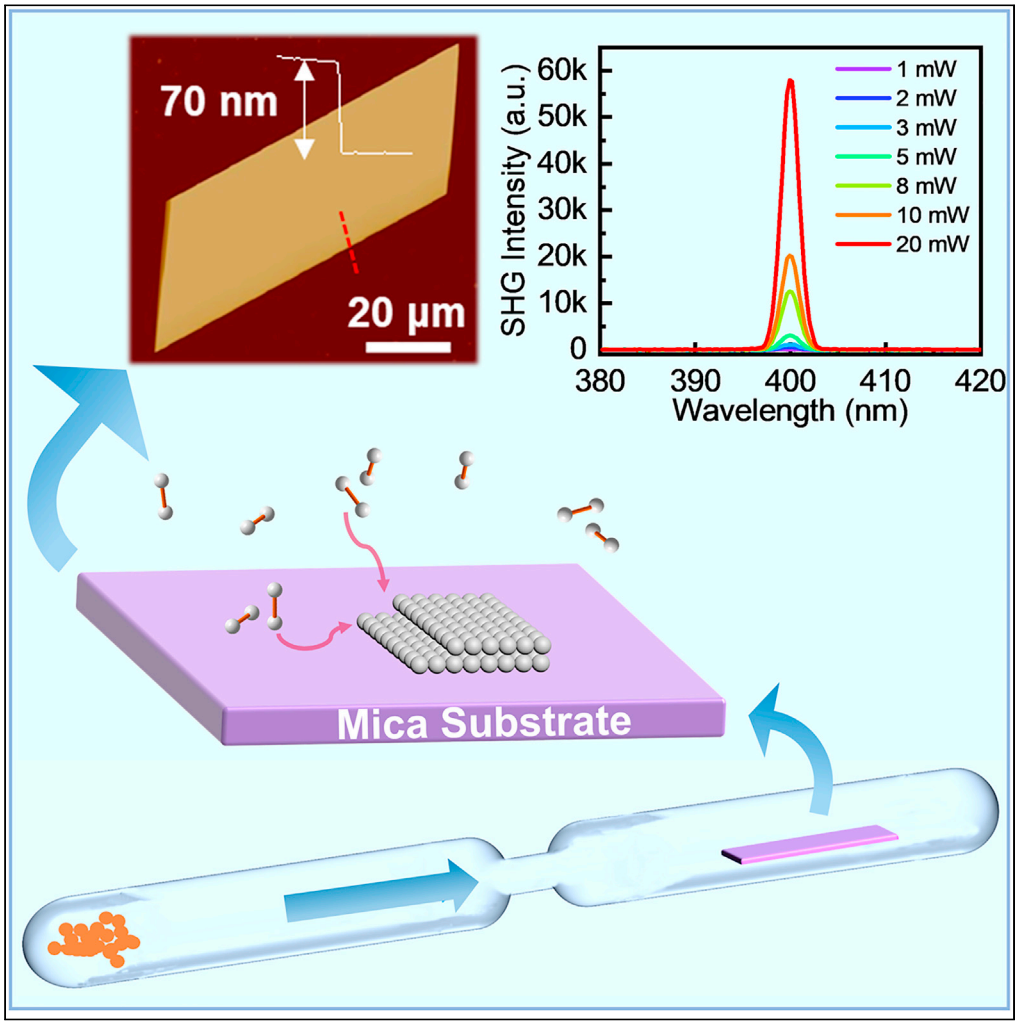

Xinxin Zhao, Jianwei Shi, Qin Yin, ..., Jie Li, Xinfeng Liu, Kai Zhang

jli2020@sinano.ac.cn (J.L.)
liuxf@nanoctr.cn (X.L.)
kzhang2015@sinano.ac.cn (K.Z.)

Highlights

High-quality 2D Te nanoflakes were directly synthesized by CVT method

The growth mechanisms of 2D Te nanoflakes were systematically studied

2D Te nanoflakes have potential applications in nonlinear optical devices

2D Te nanoflakes-based FETs exhibit high mobility of ~379 $cm^2 V^{-1} s^{-1}$

Zhao et al., iScience 25, 103594
January 21, 2022
https://doi.org/10.1016/j.isci.2021.103594

iScience

CellPress
OPEN ACCESS

Article

Controllable synthesis of high-quality two-dimensional tellurium by a facile chemical vapor transport strategy

Xinxin Zhao,[1,2,5] Jianwei Shi,[3,5] Qin Yin,[2,5] Zhuo Dong,[1,2] Yan Zhang,[1,2] Lixing Kang,[4] Qiang Yu,[2] Cheng Chen,[1,2] Jie Li,[2,*] Xinfeng Liu,[3,*] and Kai Zhang[2,6,*]

SUMMARY

Recently, as an elementary material, tellurium (Te) has received widespread attention for its high carrier mobility, intriguing topological properties, and excellent environmental stability. However, it is difficult to obtain two-dimensional (2D) Te with high crystalline quality owing to its intrinsic helical chain structure. Herein, a facile strategy for controllable synthesis of high-quality 2D Te nanoflakes through chemical vapor transport in one step is reported. With carefully tuning the growth kinetics determined mainly by temperature, tellurium nanoflakes in lateral size of up to ~40 μm with high crystallinity can be achieved. We also investigated the second harmonic generation of Te nanoflakes, which demonstrates that it can be used as frequency doubling crystals and has potential applications in nonlinear optical devices. In addition, field effect transistor devices based on the 2D Te nanoflakes were fabricated and exhibited excellent electrical properties with high mobility of 379 $cm^2 V^{-1} s^{-1}$.

INTRODUCTION

Tellurium (Te), as one of the chalcogenide elements (group VI materials), is a p-type semiconductor with a band gap of 0.34 eV, which has attracted a lot of attention for its excellent physical properties in recent years (Liu et al., 2018; Shi et al., 2020; Wang et al., 2018, 2019b; Qiu et al., 2020; Tong et al., 2020). For example, its excellent photoconductivity, high piezoelectricity, and improved thermoelectric especially excellent environmental stability provide great development potential for Te in the fields of high-performance photodetectors, field effect transistors (FETs), and thermoelectric devices (Qiu et al., 2020; Du et al., 2017; Zhang et al., 2019; Zhou et al., 2016). Tellurium atoms form helical chains along the c-axis through covalent bonds, and the helical chains are arranged in parallel by van der Waals forces in a hexagonal lattice. Thus, Te can be considered as a quasi-one-dimensional material (Li et al., 2021; Liu et al., 2018). In the past few decades, there have been more comprehensive researches on the one-dimensional (1D) structure of Te, such as nanowires, nanorods, and nanotubes (Safdar et al., 2013; Kang et al., 2019; Yin et al., 2005; Gan et al., 2020; Lee et al., 2013). However, with the continuous progress of two-dimensional (2D) material synthesis technology, more materials that are intrinsically 1D or three-dimensional structures can also be obtained in a stable 2D format. For example, Sb_2Se_3, a star photovoltaic material with the chain-like crystal structure, has successfully prepared 2D ultra-thin flakes by introducing a sodium-mediated chemical vapor deposition (CVD) growth method (Zhao et al., 2020; Mavlonov et al., 2020). Similarly, as a neotype 2D material, 2D Te has been the concern of researchers in recent years. To date, the growth of 2D Te is mainly through the solution method, but it will inevitably introduce organic matters, impurities, or defects. Some research groups have demonstrated that Te nanoflakes can also be synthesized by physical vapor deposition, van der Waals epitaxy growth, hydrogen-assisted CVD and other vapor-phase methods (Huang et al., 2017; Hussain et al., 2019; Wang et al., 2021; Zhang et al., 2019).

Furthermore, in order to achieve the controllable growth of high-quality 2D Te, we focus on the chemical vapor transport (CVT) method, an ancient technique for growing high-quality single crystals with low defect density (Legma et al., 1993; Binnewies et al., 2013). Generally, the CVT method synthesizes a bulk single crystal material first, and then the corresponding 2D material is exfoliated from the bulk counterparts (Chen et al., 2021; Wang et al., 2019a). However, the geometry and thickness of the 2D material obtained by this way cannot be well controlled, and it is difficult to get large-sized samples. Later, some research

[1]School of Nano-Tech and Nano-Bionics, University of Science and Technology of China, Hefei 230026, China

[2]CAS Key Laboratory of Nanophotonic Materials and Devices and Key Laboratory of Nanodevices and Applications, i-Lab, Suzhou Institute of Nano-Tech and Nano-Bionics (SINANO), Chinese Academy of Sciences, Suzhou 215123, China

[3]CAS Key Laboratory of Standardization and Measurement for Nanotechnology, CAS Center for Excellence in Nanoscience, National Center for Nanoscience and Technology, Beijing 100190, China

[4]Division of Advanced Materials, Suzhou Institute of Nano-Tech and Nano-Bionics (SINANO), Chinese Academy of Sciences, Suzhou 215123, China

[5]These authors contributed equally

[6]Lead contact

*Correspondence: jli2020@sinano.ac.cn (J.L.), liuxf@nanoctr.cn (X.L.), kzhang2015@sinano.ac.cn (K.Z.)

https://doi.org/10.1016/j.isci.2021.103594

groups tried to use the CVT method to grow 2D materials directly (Zhao et al., 2011). In 2017, Jiao and co-workers tried to grow 1T-$TiSe_2$ flakes by the CVT method and successfully obtained sub-10 nm $TiSe_2$ flakes with a high crystallinity (Wang et al., 2016). To further extend this method of preparing bulk material to the growth of 2D materials, they also used the same method to grow a series of large-area and high-quality 2D transition metal dichalcogenides, such as ReS_2, WS_2, MoS_2, and $Mo_xW_{1-x}S_2$ alloys (Hu et al., 2017). In addition, anisotropic 2D $ReSe_2$ was synthesized via the chemical vapor transport method in 2019, and its electron mobility is superior to CVD-grown $ReSe_2$ flakes (Xing et al., 2019). Hence, it is feasible to synthesize 2D materials directly by the CVT method instead of a crystal growth-exfoliation process, and that can be used to control and grow high-quality 2D materials. It is worth noting that most of 2D materials prepared by the CVT method in one step are layered materials at present, and there are few reports on non-layered semiconductor materials (Hu et al., 2017; Wang et al., 2019a). Owing to the limitation of tellurium quasi 1D structure, it is difficult to obtain 2D Te by mechanical exfoliation. Therefore, we attempt to directly grow high-quality and large-size 2D Te nanoflakes through the CVT method, in order to meet its application and development in different fields. This also further extends the one-step CVT method to grow non-layered 2D materials instead of a crystal growth-exfoliation process.

Herein, we successfully synthesized 2D Te nanoflakes by the CVT method in one step. By controlling the growth kinetics with temperature, we can obtain highly crystalline Te nanoflakes in lateral size of ~40 μm and thickness ~70 nm. Then, we systematically investigated the second harmonic generation (SHG) properties of the as-grown 2D Te single crystals, which indicated that Te nanoflakes can be used as frequency doubling crystals and have potential applications in nonlinear optical devices. In addition, FET devices based on 2D Te nanoflakes were also fabricated and exhibited excellent electrical properties with mobility as high as 379 $cm^2 V^{-1} s^{-1}$. The direct growth of 2D Te nanoflakes via the CVT method could be a reference for exploring the growth of other 2D materials.

RESULTS AND DISCUSSION

Preparation and material characterizations of 2D Te nanoflakes

As a traditional technique for preparing non-volatile solid crystals, chemical vapor transport has been widely used to synthesize various high-quality single-crystal bulk materials. And CVT is a process in which the source material is sealed in a vacuumed quartz ampoule and then transported and deposited through a temperature gradient formed at the source and the deposition ends. In addition, a transport agent, such as iodine, is generally added to reduce the evaporation temperature of the source materials and transport at both ends during the growth process. The transport agent can form a gaseous intermediate that is easy to combine and decompose with the source material, so the source material can be transported from one end to the other at a lower temperature (Zhao et al., 2011; Chen et al., 2021; Binnewies et al., 2013; Wang et al., 2019a). Since the CVT is transported and reacted in a closed quartz tube, oxygen and other interference factors can be better avoided, and the reaction pressure can be conveniently adjusted by temperature and the amount of the source material added. In other words, it is easier to control the reaction to be in an equilibrium state.

Taking advantages of the CVT method, the tellurium powder and mica substrate are sealed on both sides of a quartz ampoule with a neck to prepare 2D Te nanoflakes. The neck on the quartz ampoule can separate the source material from the substrate. It is worth mentioning that no transport agent was added during the growth because tellurium has a low melting point and is easy to evaporate and transport. The schematic diagram of the growth device can be seen in Figure 1A, and more information about the growth can be referred to in the method details section. Figures 1B and 1C are atomic structural models of Te. Atoms are connected by covalent bonds along the c-axis to form a spiral chain, whereas the chains are arranged in a hexagonal structure via van der Waals forces (Huang et al., 2017; Amani et al., 2018). Viewed from the x-axis direction, the zigzag layers are stacked to form a three-dimensional structure (Figure 1C). Therefore, Te is also regarded as a quasi-one-dimensional material, which is more inclined to obtain nanowires and nanorods during the growth process.

Figure 1D is an optical microscope image of 2D Te nanoflakes with a length of up to 80 μm and a width of ~20 μm, and the thickness is ~70 nm characterized by atomic force microscopy (AFM) in Figure 1E. It should be mentioned that, owing to the insufficient technology of firing the quartz ampoule, the necking diameter of the quartz ampoule we used for growth is fixed, which only plays the role of separating the substrate from the source, and cannot effectively control the transport rate. Therefore, this also hinders the further

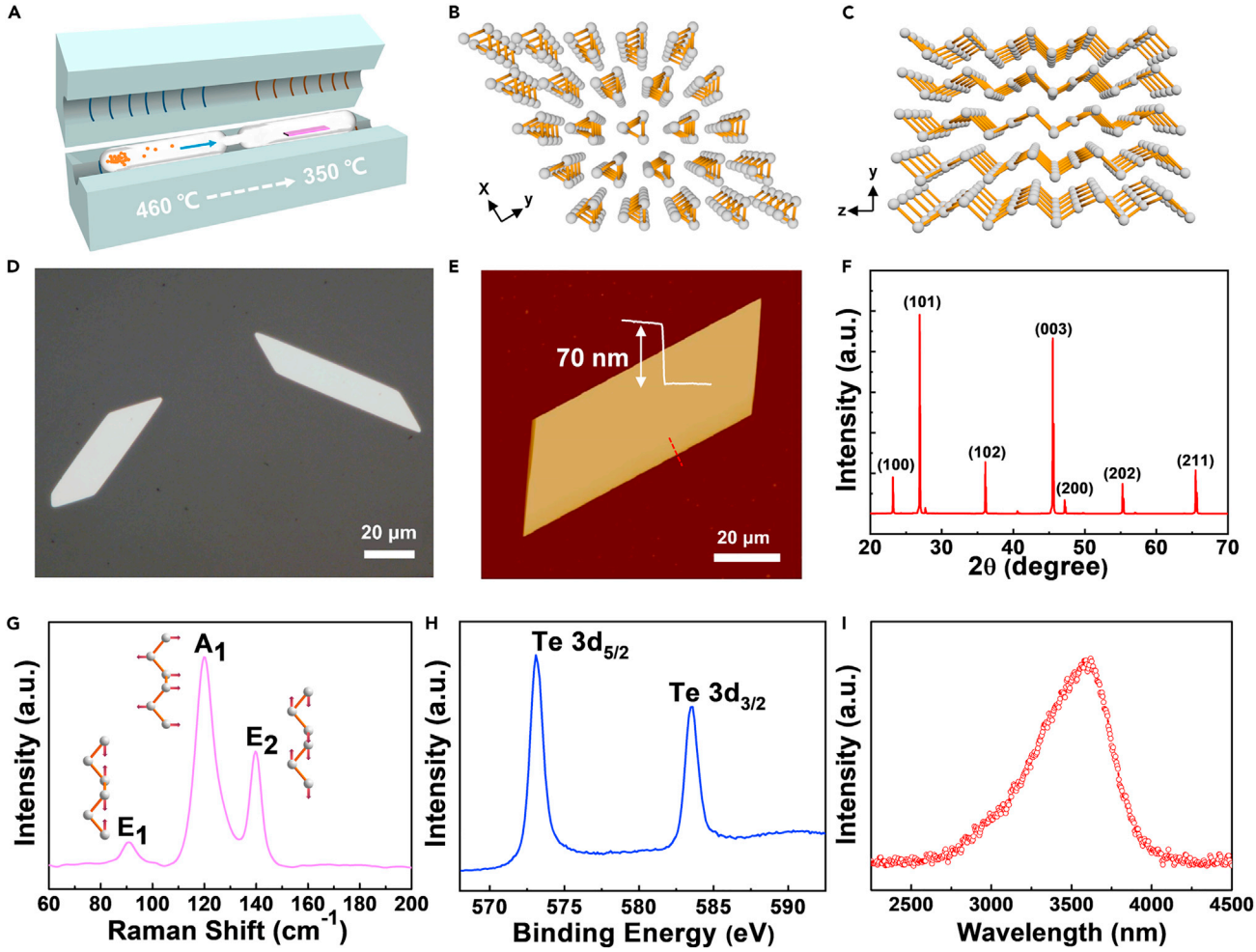

Figure 1. Synthesis of Te nanoflakes by CVT method and characterization of material

(A) Schematic diagram of CVT growth device.

(B and C) Atomic structural model of Te.

(D and E) Optical microscope and AFM images of Te nanoflakes.

(F) XRD spectra of Te nanoflakes.

(G–I) Raman, XPS, and PL spectra of CVT-grown Te nanoflakes.

adjustment of growth through dynamics and the inability to obtain thinner Te nanoflakes. By further improving the structure of the quartz ampoule or seeking other methods to control the gas transport rate, thinner 2D Te are expected. The X-ray diffraction (XRD) pattern was performed on the synthesized products, which is compatible with the standard file card (JCPDS#36-1452), as shown in Figure 1F. There are three Raman peaks of Te nanoflakes at 92, 120, and 140 cm^{-1}, corresponding to E_1, A_1, and E_2 active Raman phonon modes, respectively, which are consistent with previous reports (Zhang et al., 2019; Wang et al., 2021; Du et al., 2017). The A_1 mode is chain expansion mode and attributed to the movement of atoms on the basal plane, whereas the E_1 and E_2 modes are caused by a-axis rotation and asymmetric stretching along the c-axis, respectively (Figure 1G). In addition, X-ray photoelectron spectroscopy (XPS) was carried out to further characterize the composition of the Te nanoflakes. In Figure 1H, the Te 3d orbit was located at 573.1 and 583.5 eV, which fitted in the doublet of Te $3d_{5/2}$ and $3d_{3/2}$, respectively. There is no detected Te 3d oxidation peak, which indicates that Te nanoflakes are element crystals without obvious oxidation (He et al., 2018; Hussain et al., 2019). The photoluminescence (PL) spectrum shows a strong peak centered at 3,600 nm excited by 800 nm laser at 80 K as shown in Figure 1I, and this is also consistent with the 0.34 eV band gap of Te reported in the literature. Besides, the excellent PL properties of 2D Te nanoflakes also indicate their potential applications in optoelectronic devices.

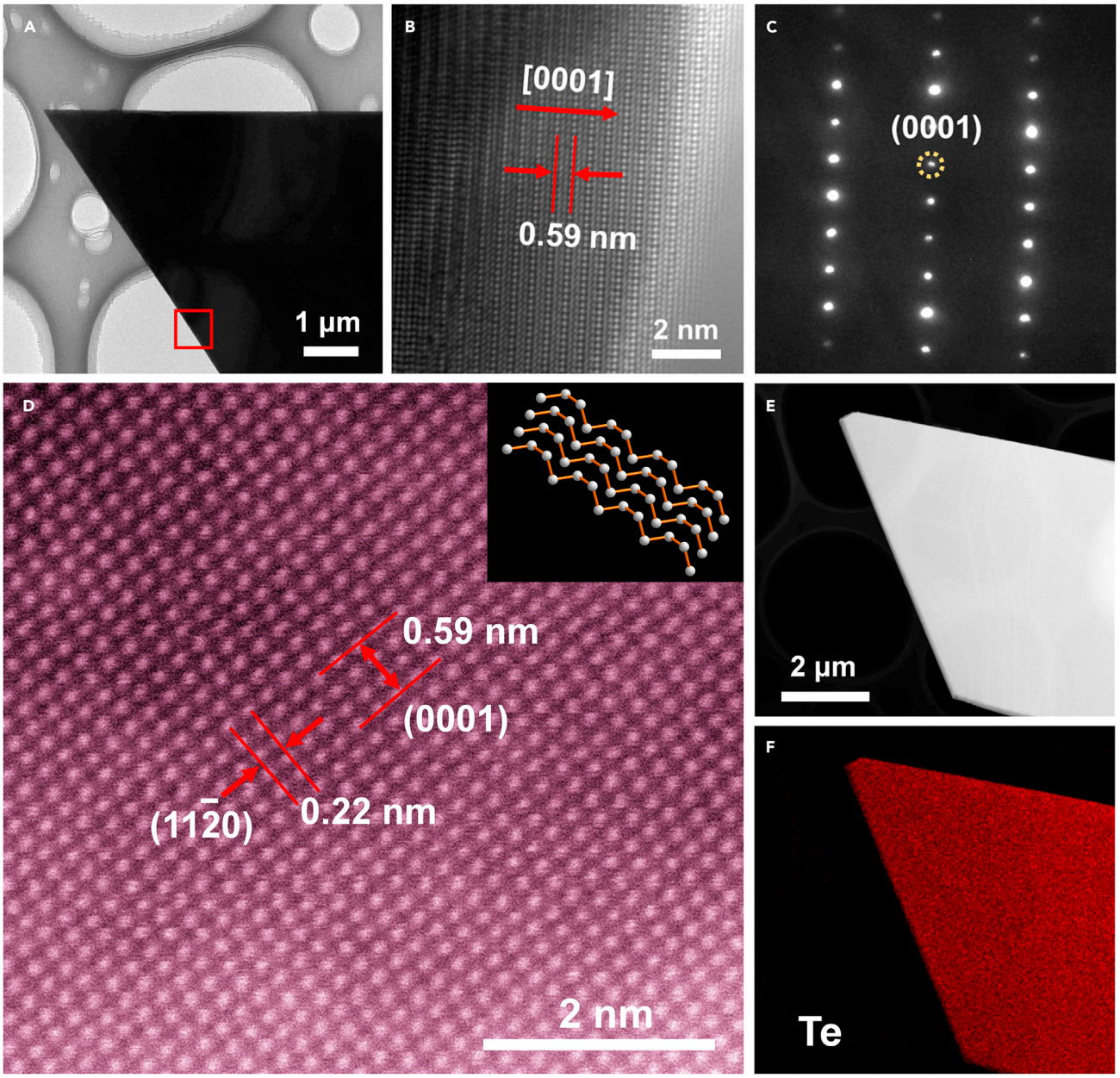

Figure 2. Atomic structure characterizations of Te nanoflakes

(A) Low-magnification bright-field TEM image of Te nanoflake.

(B and C) HRTEM image and corresponding SAED pattern obtained from the corner of Te nanoflake.

(D) Atomic-resolution HAADF-STEM image of Te nanoflake, and the inset shows the atomic model of the Te helical structure.

(E and F) Low-magnification HAADF-SETM image and EDX mapping of Te elements.

Atomic structure characterizations of 2D Te nanoflakes

Transmission electron microscopy (TEM) was performed to further reveal the atomic structure and crystal quality of as-grown 2D Te nanoflakes. Te nanoflakes synthesized on the mica substrate were dispersed in an ethanol solution by ultrasound and then transferred to a copper grid. Figure 2A is the low-resolution TEM image of Te nanoflakes, and the corresponding high-resolution TEM (HRTEM) image shows that the lattice fringe spacing is 0.59 nm, indicating that the nanoflake is growing along [0001] (Figure 2B). In addition, the selected area electron diffraction (SAED) pattern with the clear and well-arranged diffraction spots

confirms the high crystalline quality of Te nanoflakes, as shown in Figure 2C. Elemental composition of the sample is characterized by electron energy dispersive X-ray spectroscopy (EDX) in Figure S1 and proves the composition is a single elemental Te. To have a deep insight of the structure of Te nanoflakes, the atomic-scale structures are further explored by a high-angle annular dark-field scanning transmission electron microscopy (HAADF-STEM), as shown in Figure 2D. HRTEM images generally indicate the periodicity of some crystal planes, whereas HAADF-STEM images mainly reflect the incoherent signals of some atoms in the local region, so the difference between the two images is reasonable (Li et al., 2021). The direction where the lattice spacing is 0.59 nm corresponds to the (0001) crystal plane, and the interplanar spacing of 0.22 nm matches the $(11\bar{2}0)$ crystal plane. Besides, in the top inset is an atomic model indicating the helical structure of Te (Li et al., 2021). The HAADF image of Te nanoflake shown in Figure 2E, and the corresponding EDX elemental mappings, suggested homogeneous distribution of Te (Figure 2F). These results manifest that we have synthesized high-quality 2D Te by an improved one-step CVT method instead of a crystal growth-exfoliation process.

The growth mechanism of 2D Te nanoflakes

Moreover, the growth mechanism of 2D Te nanoflakes was systematically explored and analyzed. In fact, the process of growing Te nanoflakes follows the vapor-solid growth mechanism, and temperature plays a crucial role in this process (Sen et al., 2007; Hawley et al., 2012; Peng et al., 2021). Te nanoflakes were prepared in a vacuum-sealed quartz ampoule, in which supersaturation and the vapor pressure will affect Te nanostructures. Furthermore, the supersaturation and vapor pressure in the zone is determined by the temperature gradient (evaporation and deposition temperatures) (Sen et al., 2007).

When the quartz ampoule maintains a certain vapor pressure and the deposition temperature at a relatively low temperature (<350°C), more nucleation points are formed. However, owing to the low temperature of the substrate, it is difficult for Te atoms to achieve a long-range migration on the substrate (Hawley et al., 2012). And because of the characteristics of the tellurium spiral chain structure, the tellurium atoms prefer to move/grow along the longitudinal direction; lateral movement requires overcoming the high formation energy to form kinks, so it is easier to obtain 1D Te nanowires at low temperatures (Figure 3A). However, when the deposition temperature is appropriate (350°C–380°C), the energy of tellurium atoms can overcome the potential energy barrier of migration across the substrate, and the migration rate in different directions on the substrate will also become faster. In addition, the atomically smooth surface of fluorophlogopite mica as a substrate is more beneficial for Te atoms to migrate on the substrate and the growth in the manner of van der Waals epitaxy (Wang et al., 2014; Ji et al., 2016). Therefore, when the growth energy becomes high enough to overcome the formation energy required for growth in the lateral direction, Te can be epitaxially grown along multiple directions parallel to the substrate and generate 2D nanoflakes in the final, as shown in the Figure 3B. While the temperature of the source material is higher than 480°C, tellurium is evaporated rapidly to produce a high flux of Te vapor, which is in a state of high vapor pressure. If the substrate temperature is also high enough (>400°C), the mobility of tellurium atoms on the substrate is very large and the growth rate in all directions is the same since the formation energy in each direction can be overcome at this time, and spheroid Te can be obtained on the substrate (Figure 3C).

The morphology of tellurium nanostructures characterized by scanning electron microscope (SEM) under different growth temperatures is shown in Figures 3D–3F. Te nanowires with a diameter of tens of nanometers and a length of tens of microns can be obtained when the source temperature is 460°C and the deposition temperature is 330°C (Figure 3D). The structure and composition of the grown nanowires were also confirmed by TEM and Raman, and the peaks and structures were consistent with the literature (Figure S2 and Figure S3). However, when the source temperature remains unchanged and the deposition temperature is increased to 350°C, Te nanoflakes are mainly grown on the substrate. The lateral size of the nanoflakes is about 40 μm, and the thickness is about 70 nm, as shown in Figure 3E. While the source temperature and deposition temperature are 480°C and 400°C, respectively, the spherical structure with diameter of about 20 μm is obtained (Figure 3F).

Nonlinear optical properties of the as-synthesized 2D Te nanoflakes

SHG is a nonlinear optical process, in which two photons with the same frequency interact with nonlinear materials to produce one double frequency photon (Cao et al., 2020; Shi et al., 2017) as shown in Figure S4A. We explored the second-order NLO properties of as-grown Te nanoflakes and their potential

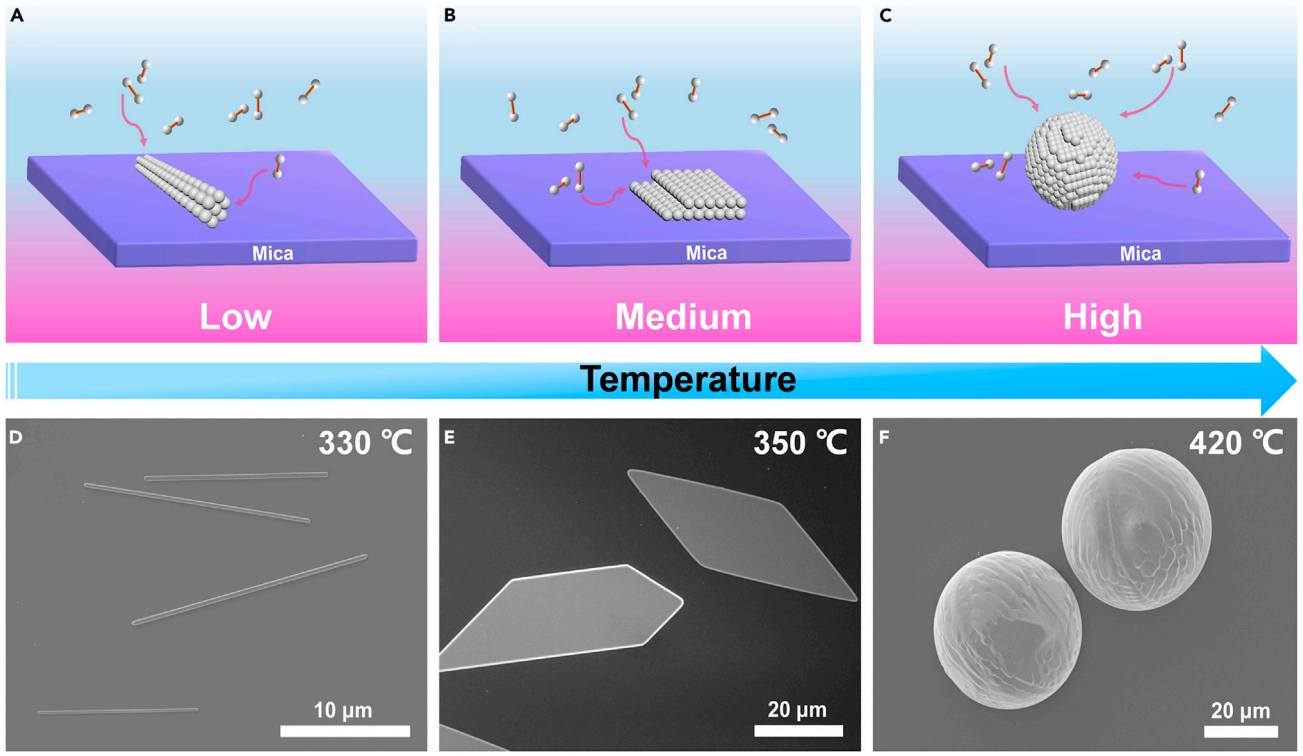

Figure 3. Morphology evolution of Te at different temperatures

(A–C) With the increase of temperature, schematic diagram of Te morphological change.

(D–F) SEM image of Te with different morphologies were obtained at (D) 330°C, (E) 350°C, and (F) 420°C, respectively.

applications in the field of optoelectronics by using a femtosecond optical parametric oscillation laser at different excitation wavelengths with a repetition rate of 80 MHz. The SHG intensity of Te nanoflakes dependence different excitation power was investigated under the excitation wavelength of 800 nm. In Figure 4A, there is a peak at 400 nm, which is the frequency doubled signal peak of the excitation wavelength. Besides, the signal intensity becomes stronger as the excitation power increases. And the pseudo-color diagram with variable power further proves this point (Figure 4B). The relationship between the excitation power and SHG intensity is linearly fitted in a logarithmic coordinate system, and the fitting slope value is approximately equal to 2.0, which is the same as the theoretical value (Figure 4C). This indicates that the intensity of the second harmonic is proportional to the square of the intensity of the laser beam, which conforms to the principle of nonlinear optics (Cao et al., 2020; Shi et al., 2017; Wang et al., 2021). Figure 4D displays the changed trend of the SHG intensity of Te nanoflakes as the excitation wavelength increases from 760 to 980 nm, and the strongest intensity is at 800 nm. In addition, the SHG mapping with uniform distribution also verifies that Te nanoflakes have high crystal quality (Figures S4B and S4C).

Electrical properties of field effect transistors based on 2D Te nanoflakes

Furthermore, we conducted the electrical properties of 2D Te nanoflakes through transferring the Te nanoflakes from mica to 285 nm SiO_2/Si substrate and fabricate back-gate FETs. Figures 5A and 5B are the output and the transfer characteristic curves of the Te nanoflake FET at room temperature, respectively. Figure 5A is the output characteristics of the device and displays the linear response of drain-source current (I_{ds}) to drain-source voltage (V_{ds}) under different gate voltages (V_g, ranging from −30 to 30 V with steps of 30 V), indicating a better gate-controlled performance, and the inset is a SEM image of the Te FET device. The corresponding transfer characteristic curve (Figure 5B) exhibits a *p*-type transport behavior, and the calculated mobility is expected to be 379 $cm^2\ V^{-1}\ s^{-1}$. This value is comparable with or even better than other methods of preparing Te. The work function of 2D Te nanoflakes on the gold substrate was explored using Kelvin probe force microscopy (KPFM) additionally, as shown in Figure S5 of supplemental information. In order to understand more about the physical properties of the device, the cool-down

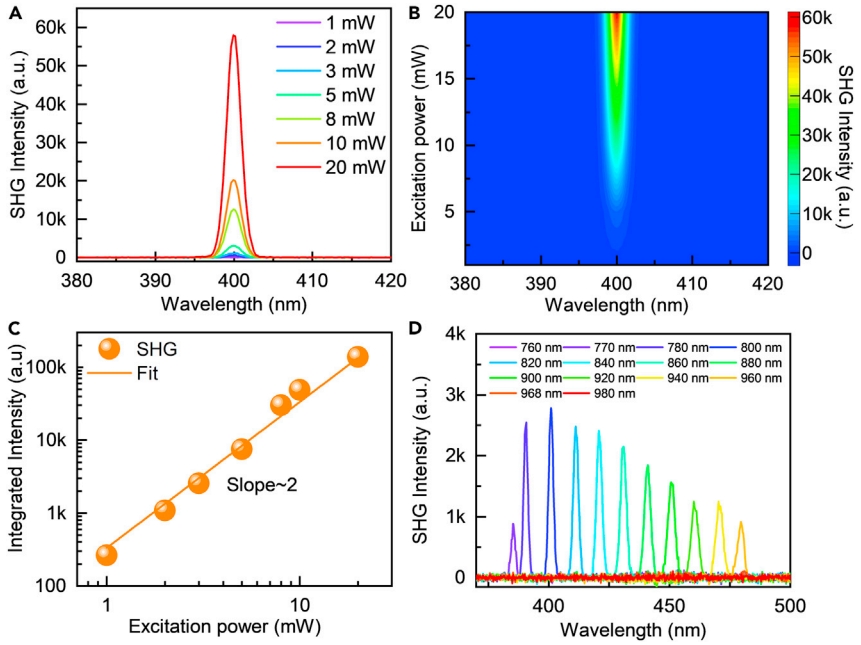

Figure 4. Nonlinear optical properties of the as-synthesized Te nanoflakes

(A) Excitation power-dependent SHG spectra.

(B) Pseudo-color diagram of variable power.

(C) Linear fitting of excitation power and SHG intensity in logarithmic coordinate.

(D) SHG intensity of Te nanoflake under varied excitation wavelengths from 760 to 980 nm.

measurements were also carried out. Figure 5C shows the relationship between temperature and resistance, and the resistance increases as the temperature decreases, showing a typical behavior of semiconductor, which is consistent with the literature. In addition, we fit the curve with Arrhenius plot in the temperature range of 150 ~ 300 K,

$$\ln R = \ln R_{\infty} + \frac{E_a}{2k_B T}$$

where E_a is the activation energy, k_B is the Boltzmann constant, R and R_∞ are the resistance when the temperature is T K and $T = \infty$, respectively. And according to the fitting curve of ln$R$ versus 1/T, the activation energy (E_a) can be calculated as 85.7 meV, as shown in Figure 5D (Li et al., 2016).

Conclusion

In summary, Te nanoflakes with high quality were synthesized in one step through the CVT method, rather than by a two-step crystal growth-exfoliation process. With this approach, the controllable synthesis of 2D Te nanoflakes has been realized. Moreover, the prepared Te nanoflakes revealed high crystallinity, and by carefully adjusting the temperature to tune the growth kinetics, Te nanoflakes with a lateral size of 45 μm and thickness about 70 nm can be obtained. Then, we further investigated the SHG effect of Te nanoflakes, which can be used as a potential two-dimensional frequency doubling crystal. In addition, the FET devices of Te nanoflakes also show excellent electrical properties. Since the CVT method has been widely applied for the mass growth of high-quality single crystals, we expect that, with adjusting the growth parameters, other 2D materials can also be grown by this method. Therefore, this will greatly promote the preparation and application research of new 2D materials.

Limitations of the study

In this work, we synthesized Te nanoflakes through the CVT method in one step. However, the thickness of the obtained Te nanoflakes is still unsatisfactory, and the growth mechanism lacks corresponding theoretical calculation. The preparation of thinner and controllable-sized Te nanoflakes by the CVT method needs further research in the future. In addition, owing to the limitations of our device

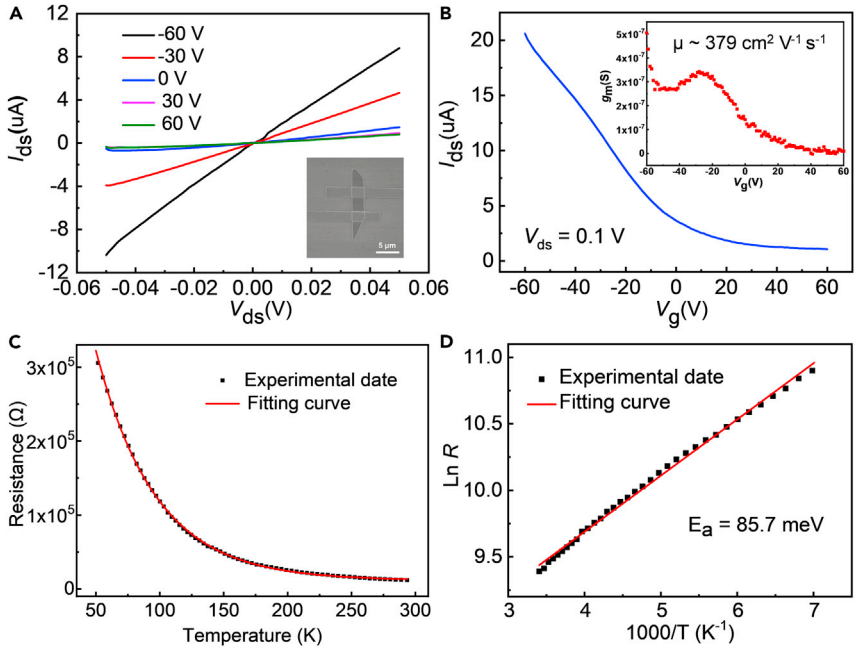

Figure 5. Electrical properties of field effect transistors based on Te nanoflakes

(A) I_{ds}–V_{ds} curves for the Te nanoflake at various different gate voltages, and the inset is a SEM image of the Te FET device.

(B) Transfer characteristic curves for Te nanoflake. The inset is the g_m versus V_g plot pictures obtained by one derivative of the transition characteristic curve.

(C) Temperature dependence resistance of Te nanoflake.

(D) ln*R* as the function of 1,000/*T*.

preparation technology, we did not measure the carrier concentration of Te nanoflakes, which still needs to be improved.

STAR★METHODS

Detailed methods are provided in the online version of this paper and include the following:

- KEY RESOURCES TABLE
- RESOURCE AVAILABILITY
  - Lead contact
  - Materials availability
  - Data and code availability
- EXPERIMENTAL MODEL AND SUBJECT DETAILS
- METHOD DETAILS
  - Synthesis of Te nanoflakes
  - Characterizations of Te nanoflakes
  - Transfer 2D Te to the target substrates
  - Nonlinear optical performance measurements
  - Devices fabrication and measurements
- QUANTIFICATION AND STATISTICAL ANALYSIS

SUPPLEMENTAL INFORMATION

Supplemental information can be found online at https://doi.org/10.1016/j.isci.2021.103594.

ACKNOWLEDGMENTS

This work was supported by the National Natural Science Foundation of China (Grant No. 61922082, 61875223, 61927813). X.L. thanks the support of the Strategic Priority Research Program of Chinese

Academy of Sciences (XDB36000000), the Ministry of Science and Technology (2017YFA0205004), the National Natural Science Foundation of China (20173025, 22073022, and 11874130), the CAS Instrument Development Project (No. Y950291), the DNL cooperation Fund, CAS (DNL202016). The support from the Vacuum Interconnected Nanotech Workstation (Nano-X) of Suzhou Institute of Nano-tech and Nano-bionics (SINANO), Chinese Academy of Sciences is also acknowledged.

AUTHOR CONTRIBUTIONS

K.Z. conceived and supervised this work. X.Z. and Q.Y. carried out the experiments of growth and material characterization. J.S. and X.L. implemented nonlinear optical performance measurements. Z.D. and Y.Z. performed the electrical properties characterization. L.K., Q.Y., and C.C. provided pertinent suggestions and assistance in data analysis and measurement. X.Z. fabricated the FET devices and wrote this manuscript. J.L. participated in the analysis of the measurements data and revised the manuscript. All authors discussed the results and commented on the manuscript.

DECLARATION OF INTERESTS

The authors declare no competing interests.

Received: August 30, 2021
Revised: November 10, 2021
Accepted: December 3, 2021
Published: January 21, 2022

REFERENCES

Amani, M., Tan, C., Zhang, G., Zhao, C., Bullock, J., Song, X., Kim, H., Shrestha, V.R., Gao, Y., Crozier, K.B., et al. (2018). Solution-synthesized high-mobility tellurium nanoflakes for short-wave infrared photodetectors. ACS Nano. *12*, 7253–7263.

Binnewies, M., Glaum, R., Schmidt, M., and Schmidt, P. (2013). Chemical vapor transport reactions - a historical review. Z. für anorganische allgemeine Chem. *639*, 219–229.

Cao, F., Zheng, S., Liang, J., Li, Z., Wei, B., Ding, Y., Wang, Z., Zeng, M., Xu, N., and Fu, L. (2020). Growth of 2D MoP single crystals on liquid metals by chemical vapor deposition. Sci. China Mater. *64*, 1182–1188.

Chen, C., Li, C., Yu, Q., Shi, X., Zhang, Y., Chen, J., Liu, K., He, Y., and Zhang, K. (2021). Bandgap opening in layered gray arsenic alloy. APL Mater. *9*, 041102.

Du, Y., Qiu, G., Wang, Y., Si, M., Xu, X., Wu, W., and Ye, P.D. (2017). One-dimensional van der Waals material tellurium: Raman spectroscopy under strain and magneto-transport. Nano Lett. *17*, 3965–3973.

Gan, X., Li, J., Xu, M., Wang, X., Liu, Z., and Zhao, J. (2020). Giant and anisotropic nonlinear optical responses of 1D van der Waals material tellurium. Adv. Opt. Mater. *8*, 2001273.

Hawley, C.J., Beatty, B.R., Chen, G., and Spanier, J.E. (2012). Shape-controlled vapor-transport growth of tellurium nanowires. Cryst. Growth Des. *12*, 2789–2793.

He, Z., Hassan, M., Ju, H.-X., Wang, R., Wang, J.-L., Chen, J.-F., Zhu, J.-F., Liu, J.-W., and Yu, S.-H. (2018). Stability and protection of nanowire devices in air. Nano Res. *11*, 3353–3361.

Hu, D., Xu, G., Xing, L., Yan, X., Wang, J., Zheng, J., Lu, Z., Wang, P., Pan, X., and Jiao, L. (2017). Two-dimensional semiconductors grown by chemical vapor transport. Angew. Chem. Int. Ed. Engl. *56*, 3611–3615.

Huang, X., Guan, J., Lin, Z., Liu, B., Xing, S., Wang, W., and Guo, J. (2017). Epitaxial growth and band structure of Te film on graphene. Nano Lett. *17*, 4619–4623.

Hussain, N., Rafique, M., Anwar, T., Murtaza, M., Liu, J., Nosheen, F., Huang, K., Huang, Y., Lang, J., and Wu, H. (2019). A high-pressure mechanism for realizing sub-10 nm tellurium nanoflakes on arbitrary substrates. 2D Mater. *6*, 045006.

Ji, J., Song, X., Liu, J., Yan, Z., Huo, C., Zhang, S., Su, M., Liao, L., Wang, W., Ni, Z., et al. (2016). Two-dimensional antimonene single crystals grown by van der Waals epitaxy. Nat. Commun. *7*, 13352.

Kang, S., Dai, T., Dang, S., Ma, X., Wang, G., Li, H., Hu, P., Yu, F., Zhou, X., Wu, S., et al. (2019). Broadband photoresponse of tellurium nanorods grown by molecular beam epitaxy. Chem. Phys. Lett. *729*, 49–53.

Lee, T.I., Lee, S., Lee, E., Sohn, S., Lee, Y., Lee, S., Moon, G., Kim, D., Kim, Y.S., Myoung, J.M., et al. (2013). High-power density piezoelectric energy harvesting using radially strained ultrathin trigonal tellurium nanowire assembly. Adv. Mater. *25*, 2920–2925.

Legma, J.B., Vacquier, G., and Casalot, A. (1993). Chemical-vapor transport of molybdenum and tungsten diselenides by various transport agents. J. Cryst. Growth *130*, 253–258.

Li, C., Zhang, L., Gong, T., Cheng, Y., Li, L., Li, L., Jia, S., Qi, Y., Wang, J., and Gao, Y. (2021). Study of the growth mechanism of solution-synthesized symmetric tellurium nanoflakes at atomic resolution. Small *17*, e2005801.

Li, L., Wang, W., Gan, L., Zhou, N., Zhu, X., Zhang, Q., Li, H., Tian, M., and Zhai, T. (2016). Ternary Ta_2NiSe_5 flakes for a high-performance infrared photodetector. Adv. Funct. Mater. *26*, 8281–8289.

Liu, Y., Wu, W., and Goddard, W.A., III (2018). Tellurium: Fast electrical and atomic transport along the weak interaction direction. J. Am. Chem. Soc. *140*, 550–553.

Mavlonov, A., Razykov, T., Raziq, F., Gan, J., Chantana, J., Kawano, Y., Nishimura, T., Wei, H., Zakutayev, A., Minemoto, T., et al. (2020). A review of Sb_2Se_3 photovoltaic absorber materials and thin-film solar cells. Sol. Energy *201*, 227–246.

Peng, M., Xie, R., Wang, Z., Wang, P., Wang, F., Ge, H., Wang, Y., Zhong, F., Wu, P., Ye, J., et al. (2021). Blackbody-sensitive room-temperature infrared photodetectors based on low-dimensional tellurium grown by chemical vapor deposition. Sci. Adv. *7*, eabf7358.

Qiu, G., Niu, C., Wang, Y., Si, M., Zhang, Z., Wu, W., and Ye, P.D. (2020). Quantum hall effect of Weyl fermions in n-type semiconducting tellurene. Nat. Nanotechnol. *15*, 585–591.

Safdar, M., Zhan, X., Niu, M., Mirza, M., Zhao, Q., Wang, Z., Zhang, J., Sun, L., and He, J. (2013). Site-specific nucleation and controlled growth of a vertical tellurium nanowire array for high performance field emitters. Nanotechnology *24*, 185705.

Sen, S., Bhatta, U.M., Kumar, V., Muthe, K.P., Bhattacharya, S., Gupta, S.K., and Yakhmi, J.V. (2007). Synthesis of tellurium nanostructures by physical vapor deposition and their growth mechanism. Cryst. Growth Des. *8*, 238–242.

Shi, Z., Cao, R., Khan, K., Tareen, A.K., Liu, X., Liang, W., Zhang, Y., Ma, C., Guo, Z., Luo, X., et al. (2020). Two-dimensional tellurium: Progress, challenges, and prospects. Nano-Micro Lett. *12*, 1–34.

Shi, J., Yu, P., Liu, F., He, P., Wang, R., Qin, L., Zhou, J., Li, X., Zhou, J., Sui, X., et al. (2017). 3R MoS_2 with broken inversion symmetry: A promising ultrathin nonlinear optical device. Adv. Mater. *29*, 1701486.

Tong, L., Huang, X., Wang, P., Ye, L., Peng, M., An, L., Sun, Q., Zhang, Y., Yang, G., Li, Z., et al. (2020). Stable mid-infrared polarization imaging based on quasi-2D tellurium at room temperature. Nat. Commun. *11*, 2308.

Wang, D., Luo, F., Lu, M., Xie, X., Huang, L., and Huang, W. (2019a). Chemical vapor transport reactions for synthesizing layered materials and their 2D counterparts. Small *15*, e1804404.

Wang, H., Mao, Y., Kislyakov, I.M., Dong, N., Chen, C., and Wang, J. (2021). Anisotropic Raman scattering and intense broadband second-harmonic generation in tellurium nanosheets. Opt. Lett. *46*, 1812–1815.

Wang, J., Zheng, H., Xu, G., Sun, L., Hu, D., Lu, Z., Liu, L., Zheng, J., Tao, C., and Jiao, L. (2016). Controlled synthesis of two-dimensional 1T-$TiSe_2$ with charge density wave transition by chemical vapor transport. J. Am. Chem. Soc. *138*, 16216–16219.

Wang, Q., Safdar, M., Xu, K., Mirza, M., Wang, Z., and He, J. (2014). Van der Waals epitaxy and photoresponse of hexagonal tellurium nanoplates on flexible mica sheets. ACS Nano *8*, 7497–7505.

Wang, Y., Ferreira, R.D.S.B., Wang, R., Qiu, G., Li, G., Qin, Y., Ye, P.D., Sabbaghi, A., and Wu, W. (2019b). Data-driven and probabilistic learning of the process-structure-property relationship in solution-grown tellurene for optimized nanomanufacturing of high-performance nanoelectronics. Nano Energy *57*, 480–491.

Wang, Y., Qiu, G., Wang, R., Huang, S., Wang, Q., Liu, Y., Du, Y., Goddard, W.A., Kim, M.J., Xu, X., et al. (2018). Field-effect transistors made from solution-grown two-dimensional tellurene. Nat. Electron. *1*, 228–236.

Xing, L., Yan, X., Zheng, J., Xu, G., Lu, Z., Liu, L., Wang, J., Wang, P., Pan, X., and Jiao, L. (2019). Highly crystalline $ReSe_2$ atomic layers synthesized by chemical vapor transport. InfoMat *1*, 552–558.

Yin, H., Xu, Z., Bai, J., Bao, H., and Zheng, Y. (2005). Ethylenediamine assisted growth of single crystal tellurium channels. Mater. Lett. *59*, 3779–3782.

Zhang, X., Jiang, J., Suleiman, A.A., Jin, B., Hu, X., Zhou, X., and Zhai, T. (2019). Hydrogen-assisted growth of ultrathin te flakes with giant gate-dependent photoresponse. Adv. Funct. Mater. *29*, 1906585.

Zhao, Y., Su, J., Zhao, Y., Luo, P., Wang, F., Han, W., Li, Y., Zu, X., Qiao, L., and Zhai, T. (2020). Sodium-mediated epitaxial growth of 2D ultrathin Sb_2Se_3 flakes for broadband photodetection. Adv. Funct. Mater. *30*, 1909849.

Zhao, Y., Hughes, R.W., Su, Z., Zhou, W., and Gregory, D.H. (2011). One-step synthesis of bismuth telluride nanosheets of a few quintuple layers in thickness. Angew. Chem. Int. Ed. Engl. *50*, 10397–10401.

Zhou, C., Dun, C., Wang, K., Zhang, X., Shi, Z., Liu, G., Hewitt, C.A., Qiao, G., and Carroll, D.L. (2016). General method of synthesis ultrathin ternary metal chalcogenide nanowires for potential thermoelectric applications. Nano Energy *30*, 709–716.

STAR★METHODS

KEY RESOURCES TABLE

REAGENT or RESOURCE	SOURCE	IDENTIFIER
Chemical regents		
Tellurium powder	Alfa Aesar	CAS: 13494-80-9
Poly (methyl methacrylate) (PMMA)	American Polymer Standards Corporation, APSC	CAS: 9011-14-7
Acetone	Sinopharm Chemical Reagent Co., China	CAS: 67-64-1
Software and algorithms		
Origin 2018	OriginLab Corporation	https://www.originlab.com
MDI Jade 6.5	Materials Data, MDI	https://materialsdata.com/
Diamond 3.0	Crystal Impact GbR, Bonn, Germany	http://www.crystalimpact.com/

RESOURCE AVAILABILITY

Lead contact

Further information and requests for resources and materials should be directed to and will be fulfilled by the lead contact, Prof. Kai Zhang (kzhang2015@sinano.ac.cn).

Materials availability

This study did not generate new unique reagents.

Data and code availability

- All data reported in this paper will be shared by the lead contact upon request.
- This paper does not report original code. Crystal data of Te are available from the Crystallography Open Database (http://www.crystallography.net/cod/search.html) under COD ID:1011098.
- Any additional information required to reanalyze the data reported in this paper is available from the lead contact upon request.

EXPERIMENTAL MODEL AND SUBJECT DETAILS

Our study does not use experimental models typical in the life sciences.

METHOD DETAILS

Synthesis of Te nanoflakes

2D Te nanoflakes was synthesized in one step by CVT technology. Firstly, 10 mg of high-purity tellurium powder (Alfa Aesar, 99.999%) was introduction into a quartz ampoule, followed the growth substrate of fluorophlogopite mica was loaded into the other end. And there is a neck on the ampoule and separated it from the source powder. After that, the quartz ampoule was sealed under vacuum (10^{-2} Pa) and placed in a horizontal tube furnace with double temperature zone for growth. By setting the source powder side at 450°C and the substrate side at 330°C to established and maintained a temperature gradient. After a growth period of 30 min at these temperatures, the quartz ampoule was slowly cooled down to room temperature.

Characterizations of Te nanoflakes

The optical images and thickness of the Te nanoflakes were taken with optical microscopy (OM, Nikon Eclipse LV100ND microscope) and atomic force microscope (AFM, Bruker Dimension Icon 3100). In addition, scanning electron microscope (SEM, Quanta FEG 250), Raman spectroscopy (LabRAM HR800, HORIBA Jobin Yvon) with visible laser light (λ = 532 nm), PL (Ti:sapphire laser, 80fs, 80 MHz), X-ray photoelectron spectroscopy (XPS, Vacuum Interconnected Nanotech Workstation employing PHI 5000 VersaProbeII system equipped with a monochromatic Al Kα X-ray source of 1486.6 eV) and X-ray diffraction

(XRD, Bruker D8 diffractometer) were used to characterize the morphology and properties of nanoflakes. Transmission electron microscopy (TEM) images and SAED with corresponding energy dispersive X-ray spectroscopy (EDX) elemental mapping were taken from a TEM (Tecnai G2 F20 S-TWIN) instrument. Scanning transmission electron microscopy (STEM) were measured by an aberration-corrected FEI Titan Themis Z STEM equipped with a CEOS DCOR probe corrector. The work function of 2D Te nanoflakes was explored using Kelvin probe force microscopy (KPFM, Bruker Dimension Icon 3100).

Transfer 2D Te to the target substrates

Firstly, the poly (methyl methacrylate) (PMMA) film was spin-coated on the mica with Te nanoflakes and dried. Then the PMMA/Te film was immersed in deionized water and peeled off from the mica substrate by the surface tension of water. After that, the PMMA film together with Te nanoflakes were attached to the 300 nm SiO_2/Si substrate and dried at 60°C for 10 min. Finally, the PMMA layer was dissolved by soaking in acetone.

Nonlinear optical performance measurements

All SHG measurements were acquired by a mode-locked Ti:sapphire laser with 80 MHz repetition rate.

Devices fabrication and measurements

Back-gated Te FETs were fabricated on the 285 nm SiO_2/Si substrates, and electron beam lithography (EBL, JEOL JBX 5500) was used to define the source/drain patterns. An Electron-beam evaporator (Ulvac Ei-5Z) was used to deposit Cr/Au (10/80 nm) film and followed by a lift-off process. The electrical Electrical measurements were carried out by a Sussmicrotec probe station (equipped with a Keithley 4200 semiconductor parameter analyzer).

QUANTIFICATION AND STATISTICAL ANALYSIS

In Figure 4C, each SHG intensity value corresponds to the average value obtained from multiple measurements of a given excitation power.